Linear instability and adiabatic fidelity for the dark state in a nonlinear atom-trimer conversion system

Shao-Ying Meng,[1,2] Li-Bin Fu,[1,3] Jing Chen,[1] and Jie Liu[1,3,4,*]

[1]*Institute of Applied Physics and Computational Mathematics, P.O. Box 8009, Beijing 100088, People's Republic of China*

[2]*Graduate School, China Academy of Engineering Physics, P.O. Box 8009-30, Beijing 100088, People's Republic of China*

[3]*Center for Applied Physics and Technology, Peking University, Beijing 100084, People's Republic of China*

[4]*College of Physics and Information Engineering, Hebei Normal University, Shijiazhuang 050016, People's Republic of China*

(Received 11 November 2008; published 30 June 2009)

We investigate the linear instability and the adiabatic fidelity of a dark state in a nonlinear atom-trimer conversion that is implemented by a stimulated Raman adiabatic passage (STIRAP). We find that the interparticle interactions could induce the instability of the atom-trimer dark state in some parameter regimes. We also discuss the adiabatic evolution of the dark state in terms of a newly defined adiabatic fidelity. Based on our theoretical analysis, we propose a feasible two-photon STIRAP scheme that has high adiabatic fidelity, less instability, and therefore could yield high atom-trimer conversion efficiency.

DOI: 10.1103/PhysRevA.79.063415 PACS number(s): 37.10.De, 37.10.Mn, 37.10.Vz

I. INTRODUCTION

The creation of ultracold molecules has opened up new possibilities for studies on molecular matter waves [1–4], strongly interacting superfluids [5], high-precision molecular spectroscopy [6], and coherent molecular optics [7]. In an atomic Bose-Einstein condensate (BEC) and a degenerate Fermi-Fermi [8] or Fermi-Bose mixture [9], a magnetic Feshbach resonance [10] or an optical photoassociation (PA) [11] technique has been used to create not only diatomic molecules but also more complex molecular condensates [12,13]. There, the efficiency of converting ultracold atoms into stable tightly bounded molecules is one of the most concerned issues. The stimulated Raman adiabatic passage (STIRAP) [14–18] in PA has been suggested to be an effective way to create ground-state molecules, taking the advantage of the coherent population trapping (CPT) state or dark state [19,20]. In the adiabatic evolution process of the dark state, the population on the excited molecular state is negligible; hence, the population losses in the excited state are suppressed effectively.

However, different from the traditional STIRAP in an Λ-atomic system, the atom-molecule STIRAP contains nonlinearities that stem from the mean-field treatment of the interparticle interactions and the conversion process of atoms to molecules. The existence of these nonlinearities make it difficult to analyze the adiabaticity of the atom-molecule conversion systems because of the absence of the superposition principle. On the other hand, the nonlinear interparticle collisions could also bring forth linear instability in certain regions of the parameter space [21–25], which is driven by the emergence of the complex intrinsic frequencies of the system. In the STIRAP, the linear instability could make the quantum evolution deviate from the dark state rapidly even in adiabatic limit [17]. Therefore, it is important to avoid such instability for the success of the STIRAP.

On the other aspect, the adiabatic theory for nonlinear quantum systems, i.e., the systems governed by the nonlinear Schrödinger equation, was first discussed in [26], where adiabatic conditions and adiabatic invariants were obtained through casting the nonlinear Schrödinger equation into an effective classical Hamiltonian. Recently, Pu *et al.* [27] and Ling *et al.* [28] extended the above adiabatic theory to the atom-dimer conversion system by linking the nonadiabaticity with the population growth in the collective excitations of the dark state. An improved adiabatic condition was put forward by Itin and Watanabe [29] via applying methods of classical Hamiltonian dynamics. The above analysis of adiabaticity and instability is mainly restricted to the atomic or hybrid atom-dimer BEC systems [26–29]. Recently, the atom-molecule dark-state technique in the STIRAP is theoretically generalized to create more complex homonuclear or heteronuclear molecule—trimer or tetramer [30–33]. Therefore, it is worthwhile to study the instability and the adiabatic property of the dark state in such complex systems.

In the present paper, we include the nonlinear interparticle collisions and focus on the linear instability induced by the collisions and the adiabatic fidelity of the atom-trimer dark state in the STIRAP. We implement the atom-trimer STIRAP via two-photon photoassociation schemes, where atoms are first photoassociated with excited dimers, and the dimers are then coupled with another atom by the second optical field to form the bound trimer molecules. We consider two schemes to implement STIRAP. In the first scheme, the atom-dimer coupling Rabi frequency is constant, while the dimer-trimer coupling Rabi frequency is time dependent. In the second scheme, the atom-dimer coupling Rabi frequency is modulated, while the dimer-trimer coupling Rabi frequency is fixed. In both cases, we find that the interparticle interactions could bring forth linear instability of the atom-trimer dark state. Taking the condensate system of ^{41}K and ^{87}Rb as an example, we further plot the phase diagrams of the instability in the parameter plane. We show that the second scheme has smaller unstable regions than the first one; hence, the STIARP technique can be implemented safely in a much larger parameter range in this scheme. Moreover, we recognize that the traditional definition of the adiabatic fidelity is not applicable to atom-molecule conversion system owing to

*liu_jie@iapcm.ac.cn

the non-U(1) invariance of Hamiltonian [34,35], while the adiabatic evolution can only be thoroughly studied quantitatively by employing the quantity of the adiabatic fidelity that describes the distance between the actual evolution and the adiabatic states (i.e., dark state). We therefore properly define the adiabatic fidelity for this system. With the help of the newly defined adiabatic fidelity, we demonstrate that the second scheme has better adiabaticity and is more effective than the first one in obtaining higher atom-trimer conversion efficiency.

Our paper is organized as follows. In Sec. II, we present the model and derive the CPT state solution. In Sec. III, through casting the nonlinear Schrödinger equation into an effective classical Hamiltonian, we investigate the linear instability with analyzing the eigenvalues of the Hamiltonian-Jacobi matrix obtained via linearizing the nonlinear equations of motion at the fixed point that corresponds to the CPT state. In Sec. IV, we study the adiabaticity of the CPT state quantitatively based on a newly defined adiabatic fidelity. In Sec. V our conclusion is presented.

II. MODEL: CPT STATE

Consider the atom-trimer conversion system, where the heteronuclear timers A_2B is formed by two different reaction paths that involve intermediate dimers A_2 (path AA) and AB (path AB), respectively. By denoting the Rabi frequency of the atom-dimer (dimer-trimer) coupling optical field with λ' (Ω') and detuning δ (Δ), including s-wave scattering processes, the second quantized Hamiltonian under the rotating frame reads

$$\hat{H} = \hat{H}_0 + \hat{H}_{int} + \hat{H}_{couple}, \tag{1}$$

where

$$\hat{H}_0 = -\hbar[\delta\hat{\psi}_d^\dagger\hat{\psi}_d + (\Delta+\delta)\hat{\psi}_g^\dagger\hat{\psi}_g], \tag{2}$$

$$\hat{H}_{int} = -\hbar\sum_{i,j}\chi'_{ij}\hat{\psi}_i^\dagger\hat{\psi}_j^\dagger\hat{\psi}_j\hat{\psi}_i. \tag{3}$$

For the two paths, the coupling terms are

$$\hat{H}^{AA}_{couple} = -\hbar[\lambda'_1(\hat{\psi}_d^\dagger\hat{\psi}_a\hat{\psi}_a + \text{H.c.}) - \Omega'_1(\hat{\psi}_g^\dagger\hat{\psi}_d\hat{\psi}_b + \text{H.c.})], \tag{4}$$

$$\hat{H}^{AB}_{couple} = -\hbar[\lambda'_2(\hat{\psi}_d^\dagger\hat{\psi}_a\hat{\psi}_b + \text{H.c.}) - \Omega'_2(\hat{\psi}_g^\dagger\hat{\psi}_d\hat{\psi}_a + \text{H.c.})]. \tag{5}$$

Here and afterward, marks AA and AB label the two different paths and $\hat{\psi}_i$ and $\hat{\psi}_i^\dagger$ are the annihilation and the creation operators for state $|i\rangle$, respectively. The terms proportional to χ_{ij} represent two-body collisions with $\chi'_{ii}=4\pi\hbar a_i/m_i$ and $\chi'_{ij}=\chi'_{ji}=2\pi\hbar a_{ij}/m_{ij}$ for $i\neq j$ (a_i and a_{ij} are s-wave scattering lengths, m_i is the mass of species i, and m_{ij} is the reduced mass between states i and j) characterizing the intrastate and the interstate interaction strengths, respectively.

As in papers [16,35], considering the conservation of the total particle numbers for different species, we put Eq. (1) into the grand canonical "Hamiltonian" by adding two multiples of the conserved particle number into the Hamiltonian,

$$\hat{K} = \hat{H} - \hbar\mu_a\hat{N}_a - \hbar\mu_b\hat{N}_b, \tag{6}$$

where $\hbar\mu_a, \hbar\mu_b$ are identified as the chemical potentials of the corresponding atoms, and N_a, N_b are the operators for the total particle number of the corresponding species. For the AA path, $\hat{N}_a=\hat{\psi}_a^\dagger\hat{\psi}_a+2\hat{\psi}_d^\dagger\hat{\psi}_d+2\hat{\psi}_g^\dagger\hat{\psi}_g$ and $\hat{N}_b=\hat{\psi}_b^\dagger\hat{\psi}_b+\hat{\psi}_g^\dagger\hat{\psi}_g$, while for the AB path, $\hat{N}_a=\hat{\psi}_a^\dagger\hat{\psi}_a+\hat{\psi}_d^\dagger\hat{\psi}_d+2\hat{\psi}_g^\dagger\hat{\psi}_g$ and $\hat{N}_b=\hat{\psi}_b^\dagger\hat{\psi}_b+\hat{\psi}_d^\dagger\hat{\psi}_d+\hat{\psi}_g^\dagger\hat{\psi}_g$.

From the Hamiltonian we can easily derive the equations of motion of the unit-scaled operators. Under the mean-field approximation, i.e., $\hat{\psi}_i$ and $\hat{\psi}_i^\dagger$ are replaced with c numbers $\sqrt{n}\psi_i$ and $\sqrt{n}\psi_i^*$, where n is the density of the total particle number. For the AA path, the set of the mean-field Gross-Pitaevskii (G-P) equations is (with $\hbar=1$)

$$\begin{aligned}
i\dot{\psi}_a &= (\omega_a-\mu_a)\psi_a - 2\lambda_1\psi_a^*\psi_d,\\
i\dot{\psi}_b &= (\omega_b-\mu_b)\psi_b + \Omega_1\psi_d^*\psi_g,\\
i\dot{\psi}_d &= [\omega_d-2\mu_a-(i\gamma+\delta)]\psi_d - \lambda_1\psi_a^2 + \Omega_1\psi_b^*\psi_g,\\
i\dot{\psi}_g &= [\omega_g-(2\mu_a+\mu_b)]\psi_g - (\Delta+\delta)\psi_g + \Omega_1\psi_d\psi_b.
\end{aligned} \tag{7}$$

For the AB path, it becomes

$$\begin{aligned}
i\dot{\psi}_a &= (\omega_a-\mu_a)\psi_a - \lambda_2\psi_b^*\psi_d + \Omega_2\psi_d^*\psi_g,\\
i\dot{\psi}_b &= (\omega_b-\mu_b)\psi_b - \lambda_2\psi_a^*\psi_d,\\
i\dot{\psi}_d &= [\omega_d-(\mu_a+\mu_b)-(i\gamma+\delta)]\psi_d - \lambda_2\psi_a\psi_b + \Omega_2\psi_a^*\psi_g,\\
i\dot{\psi}_g &= [\omega_g-(2\mu_a+\mu_b)]\psi_g - (\Delta+\delta)\psi_g + \Omega_2\psi_d\psi_a.
\end{aligned} \tag{8}$$

In the above two sets of equations (7) and (8), $\omega_i=-2\Sigma_j\chi_{ij}|\psi_j|^2$, $\chi_{ii}=\chi'_{ii}n$, $\chi_{ij}=\chi'_{ij}n$, $\lambda_i=\lambda'_i\sqrt{n}$, $\Omega_i=\Omega'_i\sqrt{n}$ are the renormalized quantities and the term proportional to γ is introduced phenomenologically to simulate the loss of intermediate dimers.

To seek the CPT solution, we take $\dot{x}\approx 0$, $x=\psi_a,\psi_b,\psi_d,\psi_g$, and $\psi_d=0$ and let $N_a=2N_b=2/3$; then one can easily derive the following CPT solutions:

$$\begin{aligned}
|\psi_g^0|^2 &= \frac{k(\lambda_i/\Omega_i)^2}{3[1+k(\lambda_i/\Omega_i)^2]},\\
|\psi_a^0|^2 &= 2|\psi_b^0|^2 = \tfrac{2}{3}(1-3|\psi_g^0|^2),
\end{aligned} \tag{9}$$

where $k=4$ ($i=1$) for the AA path and $k=1$ ($i=2$) for the AB path. A consistent check using Eqs. (7) and (8) finds that the chemical potentials and the two-photon resonance conditions are the same for both two paths, i.e.,

$$\begin{aligned}
\mu_a &= -2(\chi_a|\psi_a^0|^2 + \chi_{ab}|\psi_b^0|^2 + \chi_{ag}|\psi_g^0|^2),\\
\mu_b &= -2(\chi_{ab}|\psi_a^0|^2 + \chi_b|\psi_b^0|^2 + \chi_{bg}|\psi_g^0|^2),
\end{aligned}$$

$$\Delta_{AA} = \Delta_{AB} = -\delta + 2(2\chi_{ag} + \chi_{bg} - \chi_g)|\psi_g^0|^2 + (4\chi_a - 2\chi_{ag} + 4\chi_{ab} - \chi_{bg})|\psi_a^0|^2. \quad (10)$$

From Eqs. (9) and (10), we can conclude that, by dynamically maintaining the two-photon resonance condition, the population can be concentrated in atomic and trimer bound states under the respective limits $\lambda/\Omega \to 0$ and $\lambda/\Omega \to \infty$.

In the following discussions, we will consider two schemes to implement the two-photon STIRAP, where a pair of atoms is first associated with the molecular dimer via PA; the dimer molecule is then photoassociated with another atom to the bound trimer molecule. In scheme (i), the atom-dimer coupling Rabi frequency λ is constant, and the dimer-trimer coupling Rabi frequency is modulated as $\Omega(t) = \Omega_0 \operatorname{sech} t/\tau$; in scheme (ii), the atom-dimer coupling Rabi frequency is controlled as $\lambda = \lambda_0 \cosh t/\tau$, and the dimer-trimer coupling Rabi frequency Ω is fixed. In both cases, $\lambda/\Omega \sim \cosh t/\tau$ satisfies $\lambda/\Omega \to 0$ as $t \to 0$ and $\lambda/\Omega \to \infty$ as $t \to \infty$, which facilitates the adiabatic coherent population transfer between atoms and trimers.

III. LINEAR INSTABILITY OF THE CPT STATE

Since the nonlinear collisions between particles may cause linear instability, making the real solution deviate away rapidly from the CPT state in the adiabatic evolution, and hence result in low atom-to-molecule conversion efficiency, it is important to avoid the occurrence of instability in the STIRAP. For this purpose, through casting nonlinear Schrödinger equation into an effective classical Hamiltonian and analyzing the eigenvalues of the Hamiltonian-Jacobi matrix obtained by linearizing the equations of motion around the fixed point that corresponds to the CPT state [26,29,36], we investigate the linear instability of the atom-trimer dark state.

By making use of the canonical transformation, we cast the grand canonical Hamiltonian in Eq. (6) under the mean-field approximation into the form of a classical one with substituting old "variables" ψ_i (complex numbers $\psi_a = x_a + iy_a$, $\psi_b = x_b + iy_b$, $\psi_d = x_d + iy_d$, $\psi_g = x_g + iy_g$) into new ones x_i and y_i [37,38]. For the AA path, the classical grand Hamiltonian is

$$\begin{aligned} K = &-\{\chi_{aa}(x_a^4 + 2x_a^2y_a^2 + y_a^4) + \chi_{bb}(x_b^4 + 2x_b^2y_b^2 + y_b^4) + \chi_{dd}(x_d^4 \\ &+ 2x_d^2y_d^2 + y_d^4) + \chi_{gg}(x_g^4 + 2x_g^2y_g^2 + y_g^4) + 2\chi_{ab}(x_a^2 + y_a^2)(x_b^2 \\ &+ y_b^2) + 2\chi_{ad}(x_a^2 + y_a^2)(x_d^2 + y_d^2) + 2\chi_{ag}(x_a^2 + y_a^2)(x_g^2 + y_g^2) \\ &+ 2\chi_{bd}(x_b^2 + y_b^2)(x_d^2 + y_d^2) + 2\chi_{bg}(x_b^2 + y_b^2)(x_g^2 + x_g^2) \\ &+ 2\chi_{dg}(x_d^2 + y_d^2)(x_g^2 + y_g^2) + \delta(x_d^2 + y_d^2) + (\Delta + \delta)(x_g^2 + y_g^2) \\ &+ 2\lambda[x_d(x_a^2 + y_a^2) + 2x_a y_a y_d] - 2\Omega[x_g(x_b x_d - y_b y_d) \\ &+ y_g(x_b y_d + y_b x_d)]\} - \mu_a[x_a^2 + y_a^2 + 2(x_d^2 + y_d^2) + 2(x_g^2 + y_g^2)] \\ &- \mu_b(x_b^2 + y_b^2 + x_g^2 + y_g^2). \end{aligned} \quad (11)$$

Here x_i are the canonical momenta, while y_i are the coordinates. They are governed by the differential equations $\dot{x}_i = \frac{\partial K}{\partial y_i}$, $\dot{y}_i = -\frac{\partial K}{\partial x_i}$. For the AB path, we can obtain a similar classical grand Hamiltonian as in Eq. (11), and it is not shown here. By setting $\dot{x}_i = \dot{y}_i = 0$, we can obtain the fixed point that corresponds to the CPT state: $x_a = |\psi_a^0|$, $y_a = 0$, $x_b = |\psi_b^0|$, $y_b = 0$, $x_d = 0$, $y_d = 0$, $x_g = |\psi_g^0|$, $y_g = 0$ with the same chemical potentials and two-photon resonance conditions in Eq. (10).

The instability of the fixed points depends on eigenvalues of the Hamiltonian-Jacobi matrix. These eigenvalues can be real, complex, or pure imaginary. Only pure imaginary eigenvalues correspond to the stable fixed points; others indicate the unstable ones. Let $x_a = z_1$, $y_a = z_2$, $x_b = z_3$, $y_b = z_4$, $x_d = z_5$, $y_d = z_6$, $x_g = z_7$, $y_g = z_8$, then elements of the Hamiltonian-Jacobi matrix can be written elegantly as $J_{ij} = \frac{(-1)^i}{2} \frac{\partial^2 K}{\partial z_i \partial z_{j\pm 1}}|_{\mathrm{CPT}}$, where i,j are, respectively, the indices of rows and columns, and the plus (subtraction) sign is for odd (even) j. Substituting the CPT state into the matrix elements, we find the Hamiltonian-Jacobi matrix J around the fixed point (CPT state) for the atom-trimer conversion system. Then we solve the eigenvalues η_i of J and obtain analytically the eigenvalues other than the zero-mode frequency of the matrix J,

$$\eta_{1,2\pm} = i\omega_{1,2\pm} = \pm \frac{i}{\sqrt{2}} \sqrt{b \pm \sqrt{b^2 - c}},$$

$$b = \zeta^2 + 2\nu^2 - 2\alpha\beta - 2\sigma\eta,$$

$$\begin{aligned} c = &4(\nu^4 - 2\alpha\beta\nu^2 - 2\sigma\eta\nu^2 + \alpha^2\beta^2 + \sigma^2\eta^2 + 2\alpha\beta\sigma\eta \\ &+ 4\chi_{aa}\beta^2\zeta|\psi_a^0|^2 + 4\chi_{bb}\zeta\eta^2|\psi_b^0|^2 + 4\chi_{gg}\zeta\nu^2|\psi_g^0|^2 \\ &+ 8\chi_{ab}\beta\zeta\eta|\psi_a^0||\psi_b^0| + 8\chi_{ag}\beta\zeta\nu|\psi_a^0||\psi_g^0| + 8\chi_{bg}\nu\xi\eta|\psi_a^0||\psi_g^0|), \end{aligned} \quad (12)$$

where $\alpha = -\beta = 2\lambda_1|\psi_a^0|$, $\sigma = \eta = -\Omega_1|\psi_g^0|$, $\nu = \Omega_1|\psi_b^0|$, and $\zeta = (4\chi_{aa} - 2\chi_{ad})|\psi_a^0|^2 + (4\chi_{ab} - 2\chi_{bd})|\psi_b^0|^2 + (4\chi_{ag} - 4\chi_{dg})|\psi_g^0|^2 - \delta$ for the AA path; while $\alpha = \lambda_2|\psi_b^0| - \Omega_2|\psi_g^0|$, $\beta = -\lambda_2|\psi_b^0| - \Omega_2|\psi_g^0|$, $\sigma = -\eta = -\lambda_2|\psi_a^0|$, $\nu = \lambda_2|\psi_a^0|$, and $\zeta = (\chi_{aa} + \chi_{ab} - 2\chi_{ad})|\psi_a^0|^2 + (\chi_{ab} + \chi_{bb} - 2\chi_{bd})|\psi_b^0|^2 + (\chi_{ag} + \chi_{bg} - 2\chi_{dg})|\psi_g^0|^2 - \delta$ for the AB path; and $\omega_{1,2\pm}$ are the intrinsic frequencies of the system, which are identical to the Bogoliubov excitation frequencies of the system. Once $\eta_{1,2\pm}$ become real or complex, the corresponding CPT state is unstable. For the two paths, we find $b = \delta^2 + \frac{2l\Omega_j^2}{3} > 0$. Here $l = 1$ $(j = 1)$ for the AA path and $l = 2$ $(j = 2)$ for the AB path. Hence the unstable regime is given by either $c < 0$ or $c > b^2$. In the absence of the nonlinear collisions, i.e., $\chi_{ij} = 0$, the eigenvalues η_i reduce to $\eta_{1,2\pm}^0 = \pm \frac{i}{\sqrt{6}} \sqrt{3\delta^2 + 2l\Omega_j^2 \pm \sqrt{9\delta^4 + 12l\Omega_j^2\delta^2}}$. We see that $\eta_{1,2\pm}^0$ are all pure imaginary for both two paths, which implies that the CPT state of the atom-trimer conversion system is always stable. Therefore, the instability is caused by the nonlinear collisions, the same as in the atom-dimer coupling system [17].

In the following discussions, we consider the special system where we have taken ^{41}K and ^{87}Rb as A and B atoms, respectively. As in Refs. [18,30] the collisional parameters are chosen as $\chi_{aa} = 3.0 \times 10^{-17}$ m^3/s,, $\chi_{bb} = 4.96 \times 10^{-17}$ m^3/s, $\chi_{ab} = 8.17 \times 10^{-17}$ m^3/s, and other collisional parameters are taken as 0.877×10^{-17} m^3/s. The condensate density n is 5×10^{20} m^{-3}. As mentioned in Sec. II, we

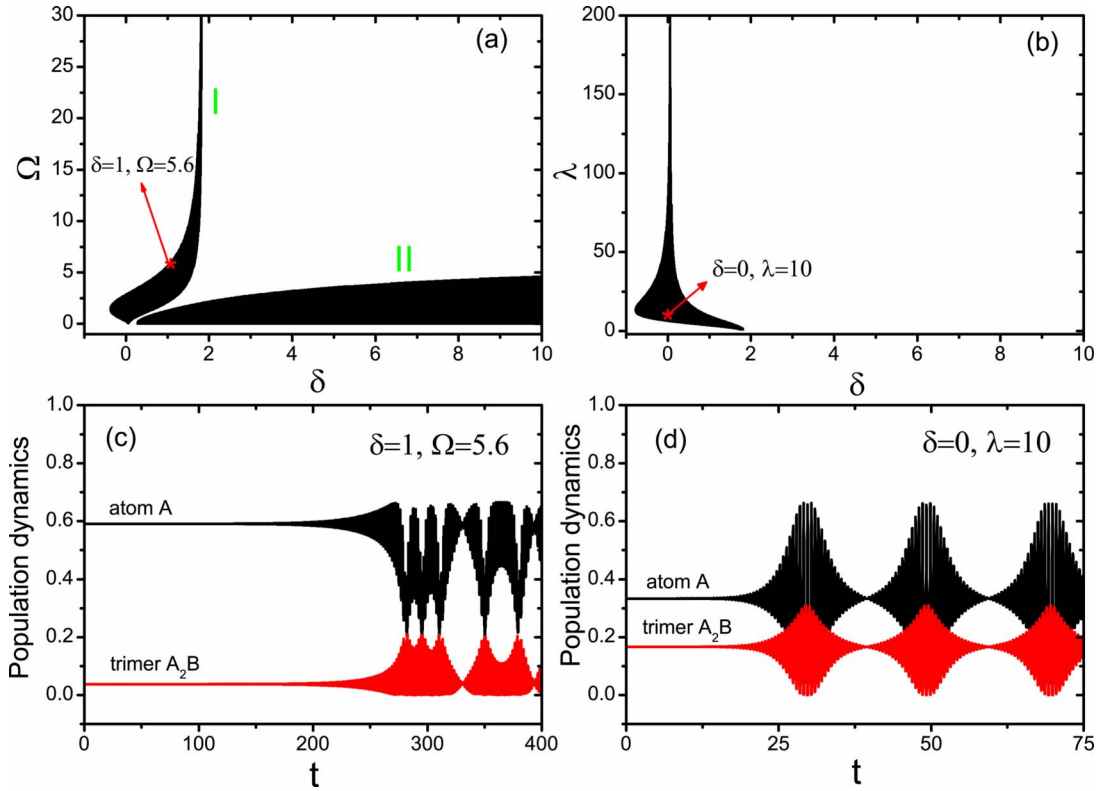

FIG. 1. (Color online) Single-path AA: [(a),(b)] instability diagrams in δ-Ω and δ-λ spaces, where the black areas correspond to the unstable regions; [(c),(d)] examples of instability in the population dynamics with the parameters labeled by $*$ in (a) and (b). Here the population dynamics of atom B and dimers are not shown. The left figures are for scheme (i), where λ is the constant Rabi frequency and $\Omega=\Omega_0$ sech t/τ is the time-dependent Rabi frequency. Time is in units of λ^{-1} (δ is in units of λ). The right figures are for scheme (ii), where $\lambda=\lambda_0$ cosh t/τ and Ω are the time-dependent and constant Rabi frequencies, respectively. Time is in units of λ_0^{-1} (δ is in units of λ_0). Other parameters are defined in Sec. III.

present two schemes to carry out the STIRAP in the atom-trimer conversion system. For scheme (i), the parameters are chosen as $\lambda=4.718\times10^4$ s^{-1}, $\Omega=\Omega_0$ sech t/τ with $\Omega_0/\lambda=20$, $\lambda\tau=20$. For scheme (ii), the parameters are chosen as $\lambda=\lambda_0$ cosh t/τ with $\lambda_0=4.718\times10^4$ s^{-1}, $\lambda_0\tau=20$, $\Omega/\lambda_0=20$. For both cases, in units of λ/n (or λ_0/n), it can be easily obtained the collisional parameters $\chi_{aa}=0.3214$, $\chi_{bb}=0.5303$, $\chi_{ab}=0.8731$, and other collisional parameters are 0.0938.

In Figs. 1(a) and 1(b), we plot the instability diagrams of schemes (i) and (ii) for the AA path, respectively, where the black (white) areas are the unstable (stable) regions. For scheme (i), the unstable region consists of two branches, namely, regions I and II [see Fig. 1(a)]. Region I corresponds to the unstable region obtained by setting $c>b^2$, whose width shrinks as Ω increases; region II is the unstable region obtained by setting $c<0$, whose width becomes fat with increasing δ. When $\delta=3$, the dynamics of the system is unstable once $0<\Omega<2.75$. That is why the population dynamics deviate from the CPT solution as Ω decreases to 2.75 at the latter stage of evolution in the recent work [30] (Fig. 1 with $\delta=3$). For scheme (ii), the unstable region only has one branch, bounded by $c=b^2$ [see Fig. 1(b)]. Its width shrinks in both directions with increasing λ or δ. By comparing Fig. 1(a) with Fig. 1(b), we find that scheme (i) has a larger unstable region than that of scheme (ii). Therefore, the STIRAP technique can be carried out safely in a much larger parameter range for the second scheme case.

Figures 1(c) and 1(d) show samples of the occurrence of instability with the parameters (labeled by $*$) in the unstable regions. In Fig. 1(c), the instability takes place at about $t=260$, while it occurs at about $t=25$ in Fig. 1(d). This time difference is caused by the different values of the real parts of the eigenvalues of the Hamiltonian-Jacobi matrix J. As has been seen in Eq. (12), the real parts of the eigenvalues η_i of the Hamiltonian-Jacobi matrix correspond to the imaginary parts of the collective excitation spectrums ω_i, i.e., $\mathrm{Re}[\eta_i]=\mathrm{Im}[\omega_i]=\alpha_i$. The nonzero imaginary parts ($\alpha_i\neq0$) of the collective excitation spectrums will bring exponential growth $e^{\alpha_i t}$ to the probability amplitudes of wave functions in the collective excitation modes and hence induce instability in dynamics of the system. Therefore, the larger the α is, the shorter the time it takes to bring forth the instability. In Fig. 1(c), $\alpha=0.03528$. In Fig. 1(d), $\alpha=0.39564$. That is why the former needs much longer time to cause instability than the latter. Based on the above analysis, we find that, when one implements the STIRAP, the occurrence of instability not only depends on the emerge of real or complex eigenvalues of the Hamiltonian-Jacobi matrix, but it also has a relation with the scanning rate of the parameters. In the STIRAP, if the parameters are swept into the unstable regions where the real parts of the eigenvalues of the Hamiltonian-Jacobi ma-

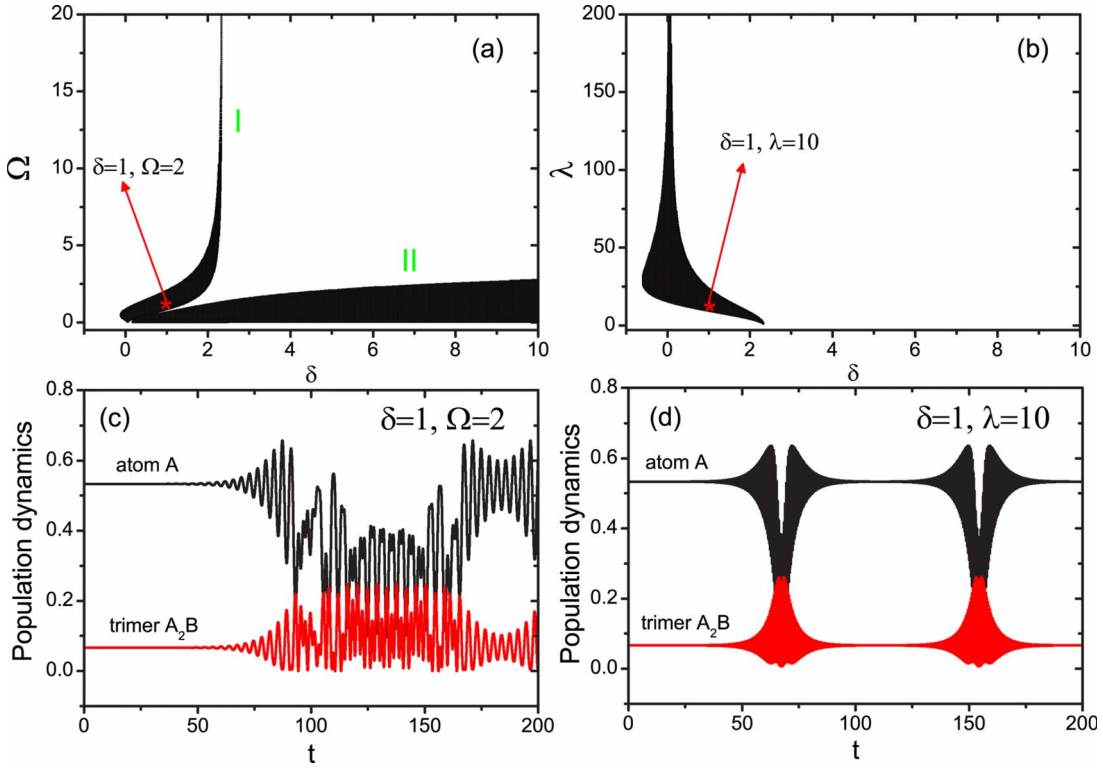

FIG. 2. (Color online) Single-path AB: [(a),(b)] instability diagrams in δ-Ω and δ-λ spaces. Here the black areas are the unstable regions; [(c),(d)] examples of instability in population dynamics with the parameters labeled by $*$ in (a) and (b). Here the population dynamics of atom B and dimers are not shown. The external fields and the parameters in (a) and (b) are the same as in Figs. 1(a) and 1(b), respectively.

trix are very small but the scanning speed of parameters is relatively fast, then the instability may not have enough time to happen as the parameters are scanned into the stable region. Here even if the real or complex eigenvalues of the Hamiltonian are present, the instability does not take place. This has not been discussed before.

For the AB path, the instability diagrams and examples of the occurrence of instability for schemes (i) and (ii) are shown in Figs. 2(a) and 2(c) and Figs. 2(b) and 2(d), respectively. And we can obtain the similar conclusions as in the AA path, i.e., the second scheme has smaller unstable regions than the first one; hence, the STIRAP technique can be implemented in a much larger parameter range in this scheme.

For both paths AA and AB, one can see that the linear instability may occur with the increasing of detuning δ for small Ω in scheme (i), while it will not take place as δ grows in scheme (ii). Therefore, the second scheme is more feasible for experimental manipulation of the coherent conversion of an atomic BEC into a molecular BEC via STIRAP. This big difference between the two schemes predicted by our theory should be observable in experiments.

IV. ADIABATIC FIDELITY OF THE CPT STATE

In the stable region, the existence of the CPT state facilitates the adiabatic coherent population transfer between atoms and trimers. However, owing to the invalidation of the superposition principle in this nonlinear system, it is not justified to apply the adiabatic condition of quantum mechanics to study the adiabatic evolution of the CPT state. In fact, the adiabatic evolution of a system can be thoroughly studied quantitatively by employing the adiabatic fidelity which describes the distance between the adiabatic solution and the actual one. However, for the atom-trimer conversion system, the traditional definition of fidelity is no longer suitable because the system is not invariant under the U(1) transformation. Therefore, we should properly define the fidelity for this system, as in recent papers [34,35]. Mathematically, we see that the Hamiltonians of the two paths in the atom-trimer conversion system are invariant under the following transformation:

$$U(\phi) = e^{i\Theta(\phi)}, \tag{13}$$

where

$$\Theta(\phi) = \begin{pmatrix} \phi_a & 0 & 0 & 0 \\ 0 & \phi_b & 0 & 0 \\ 0 & 0 & \phi_d & 0 \\ 0 & 0 & 0 & 2\phi_a + \phi_b \end{pmatrix}, \tag{14}$$

where $\phi_d = 2\phi_a$ for the AA path and $\phi_d = \phi_a + \phi_b$ for the AB path. Under this transformation, $|\psi\rangle = (\psi_a, \psi_b, \psi_d, \psi_g)^T \rightarrow |\psi'\rangle = U(\phi)|\psi\rangle$. This two states represent the same state, which requires that the definition of fidelity should not only make the distance between $|\psi\rangle$ and itself to be 1, but also the distance between $|\psi\rangle$ and $|\psi'\rangle$ to be 1. For convenience, we denote the fidelity of two states $|\psi_1\rangle$ and $|\psi_2\rangle$ as $f(|\psi_1\rangle, |\psi_2\rangle)$.

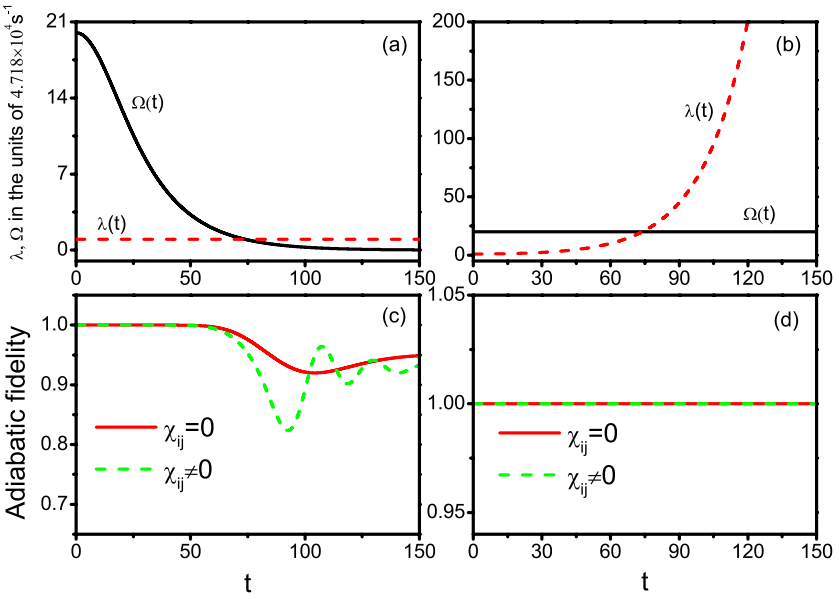

FIG. 3. (Color online) Single-path AA: [(a),(b)] Rabi frequencies and [(c),(d)] adiabatic fidelity as functions of time with and without nonlinear collisions for $\delta=-3$, $\gamma=0$. The left figures are for scheme (i), where $\Omega=\Omega_0$ sech t/τ and λ is fixed. Time is in units of λ (δ,γ is in units of λ). The right figures are for scheme (ii), where $\lambda=\lambda_0$ cosh t/τ and Ω is fixed. Time is in units of λ_0 (δ is in units of λ_0). Other parameters are defined in Sec. III.

Then this definition should not only satisfy $f(|\psi\rangle,|\psi\rangle)=1$ for any $|\psi\rangle$ but also fulfill $f(|\psi\rangle,U(\phi)|\psi\rangle)=1$ for any ϕ. With this consideration, we define the fidelity for atom-trimer conversion system as

$$f(|\psi_1\rangle,|\psi_2\rangle)=|\langle\bar{\psi}_1|\bar{\psi}_2\rangle|^2, \tag{15}$$

where $|\bar{\psi}\rangle$ is the rescaled wave function of $|\psi\rangle=(\psi_a,\psi_b,\psi_d,\psi_g)^T$,

$$|\bar{\psi}\rangle=\left(\frac{\psi_a^2\psi_b}{|\psi_a||\psi_b|},\frac{\psi_a^2\psi_b}{|\psi_a^2|},\frac{\sqrt{2}\psi_j\psi_d}{|\psi_j|},\sqrt{3}\psi_g\right). \tag{16}$$

Here $j=b$ for the AA path and $j=a$ for the AB path. As in papers [34,35], it can be proved that this kind of definition satisfies the above two conditions and other conditions for fidelity definition [39]. Because we are only concerned with the adiabatic evolution of the CPT state throughout, we denote the adiabatic fidelity of the dark state as $F=|\langle\psi(t)|\overline{\mathrm{CPT}}\rangle|^2$, where $|\psi(t)\rangle$ is the exact solution of the Schrödinger equation in Eq. (7) or Eq. (8). $|\psi(t)\rangle$ and $|\overline{\mathrm{CPT}}\rangle$ are the rescaled wave functions of $|\psi(t)\rangle$ and CPT state, respectively. If the system can adiabatically evolve along the CPT state, then the value of the adiabatic fidelity should be close to 1.

Figure 3 shows the Rabi frequencies and the adiabatic fidelity of the CPT state as functions of time with and without nonlinear collisions for the single AA path. The left figures are for scheme (i), where λ is constant, while $\Omega=\Omega_0$ sech t/τ is time dependent [see Fig. 3(a)]. As can be seen in Fig. 3(c), no matter whether the interparticle interactions are considered, the magnitude of the adiabatic fidelity is about 1 at the initial time, but begins to decrease at some later time, then diminishes to the minimal value, and finally approaches to a steady value which is smaller than 1. The minimal value of the adiabatic fidelity that can be used to describe the adiabaticity of the system is close to 1. Therefore, the system can approximately evolve adiabatically along the CPT state. The right figures are for scheme (ii), where $\lambda=\lambda_0$ cosh t/τ is modulated and Ω is fixed [see Fig. 3(b)]. In this scheme, no matter whether the nonlinear collisions are included, the adiabatic fidelity is equal to 1 during the entire evolution [see Fig. 3(d)]. Therefore, the system can follow the CPT state completely. In comparison with the results in schemes (i) and (ii), we conclude that the adiabaticity of the system in the second scheme is better than the first one.

For the AB path, we obtain the similar conclusions as in the AA path by observing Fig. 4 where the time dependence of the adiabatic fidelity is shown. In practical experiments, when the parameters are chosen in the stable regions, one can observe the adiabatic fidelity stays at 1 throughout the adiabatic evolution in scheme (ii), while it departs from 1 at the middle stage of evolution in scheme (i). For example, in the AA path, the minimal value of adiabatic fidelity reaches 0.82, and the final value is 0.91 [see Fig. 3(c)]. Our theory suggests that the second scheme is more effective than the first one in obtaining higher atom-trimer conversion effi-

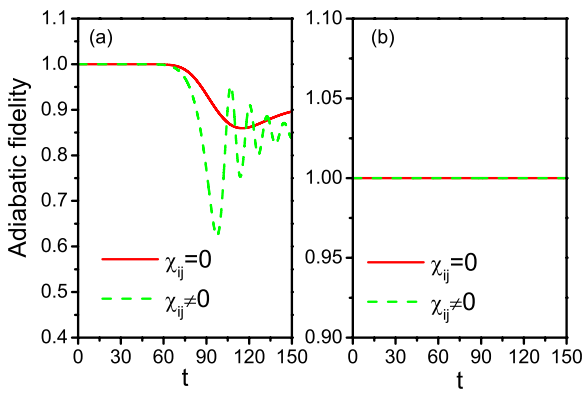

FIG. 4. (Color online) Single-path AB: adiabatic fidelity as a function of time with and without nonlinear collisions for $\delta=-3$, $\gamma=0$. In (a), the Rabi frequencies are the same as in Fig. 3(a); In (b), the Rabi frequencies are the same as in Fig. 3(b). Other parameters are the same as in Fig. 3.

ciency. This theoretical prediction waits for future experiment's test.

V. CONCLUSION

In conclusion, we investigate the linear instability and the adiabatic fidelity of the atom-trimer dark state in the STIRAP. Here the heteronuclear trimers are formed through two different paths, namely, AA and AB paths. We adopt two different schemes of two-photon photoassociation to carry out the STIRAP for these two paths. In the first scheme, the atom-dimer coupling Rabi frequency λ is constant, and the dimer-trimer coupling Rabi frequency is modulated as $\Omega(t) = \Omega_0 \operatorname{sech} t/\tau$; in the second scheme, the atom-dimer coupling Rabi frequency is controlled as $\lambda = \lambda_0 \cosh t/\tau$, and the dimer-trimer coupling Rabi frequency Ω is fixed. In both cases, we find that the interparticle interactions could bring forth linear instability in some parameter regions. We also find that the unstable regions of scheme (ii) are much smaller than scheme (i); hence, the STIRAP technique can be implemented safely in a much larger parameter range in the second scheme. In addition, the adiabatic evolution of the atom-trimer dark state is studied quantitatively in terms of a newly defined adiabatic fidelity. Our calculation suggests that the adiabaticity of dark state in the second scheme is better than that in the first scheme; hence, the second scheme is more effective than the first one in obtaining higher atom-trimer conversion efficiency.

ACKNOWLEDGMENTS

This work was supported by the National Natural Science Foundation of China (Grants No. 10725521 and No. 10604009) and the National Fundamental Research Programme of China under Grants No. 2006CB921400 and No. 2007CB814800.

[1] J. Herbig, T. Kraemer, M. Mark, T. Weber, C. Chin, H.-C. Nägerl, and R. Grimm, Science **301**, 1510 (2003).
[2] K. Xu, T. Mukaiyama, J. R. Abo-Shaeer, J. K. Chin, D. E. Miller, and W. Ketterle, Phys. Rev. Lett. **91**, 210402 (2003).
[3] S. Jochim, M. Bartenstein, A. Altmeyer, G. Hendl, S. Riedl, C. Chin, J. Hecker Denschlag, and R. Grimm, Science **302**, 2101 (2003).
[4] M. Greiner, C. A. Regal, and D. S. Jin, Nature (London) **426**, 537 (2003); M. W. Zwierlein, C. A. Stan, C. H. Schunck, S. M. F. Raupach, S. Gupta, Z. Hadzibabic, and W. Ketterle, Phys. Rev. Lett. **91**, 250401 (2003); T. Bourdel, L. Khaykovich, J. Cubizolles, J. Zhang, F. Chevy, M. Teichmann, L. Tarruell, S. J. J. M. F. Kokkelmans, and C. Salomon, *ibid.* **93**, 050401 (2004).
[5] M. Bartenstein, A. Altmeyer, S. Riedl, S. Jochim, C. Chin, J. H. Denschlag, and R. Grimm, Phys. Rev. Lett. **92**, 120401 (2004).
[6] M. Bartenstein, A. Altmeyer, S. Riedl, R. Geursen, S. Jochim, C. Chin, J. H. Denschlag, R. Grimm, A. Simoni, E. Tiesinga, C. J. Williams, and P. S. Julienne, Phys. Rev. Lett. **94**, 103201 (2005).
[7] J. R. Abo-Shaeer, D. E. Miller, J. K. Chin, K. Xu, T. Mukaiyama, and W. Ketterle, Phys. Rev. Lett. **94**, 040405 (2005).
[8] B. DeMarco and D. S. Jin, Science **285**, 1703 (1999).
[9] G. Modugno, G. Roati, F. Ferlaino, R. J. Brecha, and M. Inguscio, Science **297**, 2240 (2002).
[10] H. Feshbach, *Theoretical Nuclear Physics* (Wiley, New York, 1992).
[11] K. Bergmann, H. Theuer, and B. W. Shore, Rev. Mod. Phys. **70**, 1003 (1998).
[12] T. Kraemer, M. Mark, P. Waldburger, J. G. Danzl, C. Chin, B. Engeser, A. D. Lange, K. Pilch, A. Jaakkola, H.-C. Nägerl, and R. Grimm, Nature (London) **440**, 315 (2006).
[13] C. Chin, T. Kraemer, M. Mark, J. Herbig, P. Waldburger, H.-C. Nägerl, and R. Grimm, Phys. Rev. Lett. **94**, 123201 (2005).
[14] J. R. Kuklinski, U. Gaubatz, F. T. Hioe, and K. Bergmann, Phys. Rev. A **40**, 6741 (1989).
[15] U. Gaubatz, P. Rudecki, M. Becker, S. Schiemann, M. Kulz, and K. Bergmann, Chem. Phys. Lett. **149**, 463 (1988); U. Gaubatz, P. Rudecki, S. Schiemann, and K. Bergmann, J. Chem. Phys. **92**, 5363 (1990).
[16] M. Mackie, R. Kowalski, and J. Javanainen, Phys. Rev. Lett. **84**, 3803 (2000); Matt Mackie, Kari Härkönen, Anssi Collin, Kalle-Antti Suominen, and Juha Javanainen, Phys. Rev. A **70**, 013614 (2004); M. Mackie, A. Collin, and J. Javanainen, *ibid.* **71**, 017601 (2005).
[17] H. Y. Ling, H. Pu, and B. Seaman, Phys. Rev. Lett. **93**, 250403 (2004).
[18] P. D. Drummond, K. V. Kheruntsyan, D. J. Heinzen, and R. H. Wynar, Phys. Rev. A **65**, 063619 (2002); **71**, 017602 (2005).
[19] K. Winkler, G. Thalhammer, M. Theis, H. Ritsch, R. Grimm, and J. H. Denschlag, Phys. Rev. Lett. **95**, 063202 (2005).
[20] S. Moal, M. Portier, J. Kim, J. Dugué, U. D. Rapol, M. Leduc, and C. Cohen-Tannoudji, Phys. Rev. Lett. **96**, 023203 (2006).
[21] Biao Wu and Qian Niu, Phys. Rev. A **64**, 061603(R) (2001).
[22] Y. Nakamura, M. Mine, M. Okumura, and Y. Yamanaka, Phys. Rev. A **77**, 043601 (2008).
[23] Y. Shin, M. Saba, M. Vengalattore, T. A. Pasquini, C. Sanner, A. E. Leanhardt, M. Prentiss, D. E. Pritchard, and W. Ketterle, Phys. Rev. Lett. **93**, 160406 (2004).
[24] L. Fallani, L. De Sarlo, J. E. Lye, M. Modugno, R. Saers, C. Fort, and M. Inguscio, Phys. Rev. Lett. **93**, 140406 (2004).
[25] L. E. Sadler, J. M. Higbie, S. R. Leslie, M. Vengalattore, and D. M. Stamper-Kurn, Nature (London) **443**, 312 (2006).
[26] J. Liu, B. Wu, and Q. Niu, Phys. Rev. Lett. **90**, 170404 (2003).
[27] H. Pu, P. Maenner, W. Zhang, and H. Y. Ling, Phys. Rev. Lett. **98**, 050406 (2007).
[28] H. Y. Ling, P. Maenner, W. P. Zhang, and H. Pu, Phys. Rev. A **75**, 033615 (2007).
[29] A. P. Itin and S. Watanabe, Phys. Rev. Lett. **99**, 223903 (2007).
[30] H. Jing, J. Cheng, and P. Meystre, Phys. Rev. Lett. **99**, 133002 (2007).
[31] H. Jing and Y. Jiang, Phys. Rev. A **77**, 065601 (2008).

[32] H. Jing, J. Cheng, and P. Meystre, Phys. Rev. A **77**, 043614 (2008).
[33] H. Jing, F. Zheng, Y. Jiang, and Z. Geng, Phys. Rev. A **78**, 033617 (2008).
[34] S. Y. Meng, L. B. Fu, and J. Liu, Phys. Rev. A **78**, 053410 (2008).
[35] L. H. Lu and Y. Q. Li, Phys. Rev. A **77**, 053611 (2008).
[36] G. F. Wang, D. F. Ye, L. B. Fu, X. Z. Chen, and J. Liu, Phys. Rev. A **74**, 033414 (2006).
[37] A. Heslot, Phys. Rev. D **31**, 1341 (1985).
[38] A. P. Itin, S. Watanabe, and V. V. Konotop, Phys. Rev. A **77**, 043610 (2008).
[39] M. A. Nielsen and I. L. Chuang, *Quantum Computation and Quantum Information* (Cambridge University Press, Cambridge, England, 2000), pp. 399–424; Jing-Ling Chen, Libin Fu, Abraham A. Ungar, and Xian-Geng Zhao, Phys. Rev. A **65**, 054304 (2002); **65**, 024303 (2002).